Atmos. Meas. Tech. Discuss., 6, 4551–4575, 2013
www.atmos-meas-tech-discuss.net/6/4551/2013/
doi:10.5194/amtd-6-4551-2013

Atmospheric Measurement Techniques
Open Access
Discussions

0.355 µm direct detection wind lidar under testing during a field campaign in consideration of ESA's ADM-Aeolus Mission

S. Lolli[1,*], A. Delaval[1,], C. Loth[1], A. Garnier[2,***], and P. H. Flamant[1]**

[1]Laboratoire de Météorologie Dynamique – UMR8539, Ecole Polytechnique, Palaiseau, France
[2]Laboratoire Atmosphères, Milieux, Observations Spatiales, CNRS-UVSQ-UPMC, Guyancourt, France
[*]now at: JCET-NASA, GSFC, 20771, Greenbelt, MD, USA
[**]on leave from LMD
[***]now at: Science Systems Applications Inc/LaRC, Hampton, VA, USA

Received: 27 April 2013 – Accepted: 8 May 2013 – Published: 23 May 2013

Correspondence to: S. Lolli (simone.lolli@nasa.gov)

Published by Copernicus Publications on behalf of the European Geosciences Union.

Abstract

The atmospheric wind field information is a key issue to Numerical Weather Prediction (NWP) and climate studies. A space based Wind Doppler lidar mission so-called ADM-Aeolus is currently developed by the European Space Agency for a launch in 2015. Such a Doppler lidar will provide accurate direct measurements of horizontal wind velocity in the depth of atmosphere. The wind data will be evenly distributed at a global scale. The goal is to enhance the present meteorological observation system over sparse wind data regions, and more important to provide direct wind information in the tropics where no geostrophic wind can be derived from passive radiometer satellite. ADM-Aeolus is basically a 0.355 µm high spectral resolution backscatter lidar. This concept was under test during a field campaign conducted at the Haute Provence Observatory in France 1999. It was the opportunity to address the self-consistency of wind measurements made by different active remote sensors i.e. lidars and a 72-MHz radar, and balloon radio soundings.

1 Introduction

The atmospheric wind field is a key input to meteorology and climate studies. The world wide radio-sounding network is the backbone of the World Meteorological Organization with aircraft, buoys and meteorological radars. It remains that wind data are still sparse and unevenly distributed between land and ocean and Northern and Southern Hemispheres. Such a limitation is a major constraint to improve numerical weather prediction models (Courtier et al., 1992). Then, the satellite observations are called to increase the wind data set such as (i) scatterometers, (ii) cloud track wind and (iii) geostrophic wind derived from the mass field.

In the early 80's, a new concept of Wind lidar satellite came into discussion (Huffaker, 1984). It was based on a high-energy pulsed single mode CO_2 laser associated to a heterodyne detection. The technical constrains to develop a lidar in space led to new

Wind lidar concepts implementing a single mode doubled Nd-YAG laser and direct detection (Chanin et al., 1989). Then the technique implemented a tripled Nd-YAG laser emitting at 0.355 µm (Gentry et al., 2000; Flesia et al., 2000). This technique is the root to the European Space Agency's Atmospheric Dynamic Mission-Aeolus to be launched in 2015 for accurate wind velocity profiling in the entire troposphere and lower stratosphere. The ADM-Aeolus mission is designed to fulfill WMO requirements regarding vertical resolution and accuracy (see Stoffelen et al., 2005). The lidar Doppler technique consists in sounding the atmosphere by a single frequency pulsed laser and measuring the frequency shift due to the Doppler effect: $\Delta\nu = -2\frac{V_r}{\lambda}$, of the backscattered signal spectrum (i.e. relative motion between the instrument and particles and molecules moving with the wind). The Doppler frequency shift $\Delta\nu$ is in Hz, V_r is the radial velocity along the lidar Line of Sight (LoS), and λ the laser wavelength. Then, the horizontal velocity is $V_h = V_r \cos\theta$, were θ is the angle between the lidar LoS and the nadir direction.

Heterodyne detection technique analyzes the backscattered spectrum from aerosol or cloud particles while direct detection analyses mostly the backscattered spectrum from air molecules. The backscattered spectrum from particles is narrow: usually limited by the laser line width, while the backscattered spectrum from air molecules is broad according to molecules thermal velocity distribution (it results in so called Rayleigh–Brillouin spectrum). In heterodyne detection lidar the atmospheric signals are mixed with the beam of a local oscillator laser while direct detection lidars implement a Double Fabry–Perot etalon (Chanin et al., 1989; Korb et al., 1990; Garnier and Chanin, 1992; Gentry et al., 1994, 2000; Flesia et al., 2000). Regarding the deployment of a Doppler lidar in space, the geographical and height distribution of atmospheric particles loading has been questioned. For atmospheric molecules are uniformly distributed geographically with a known dependence in height, ESA decided to select in 1999 a spaceborne wind lidar based on molecular scattering at 0.355 µm. Such a UV wavelength increases the signal strength according to λ^{-4} law dependence and fulfills eye safety regulation.

The Wind lidar techniques, heterodyne and direct detections, were tested and validated separately in field studies. As an example see: Chanin et al. (1989, 1994); Korb et al. (1990, 1998); Garnier and Chanin (1992); Gentry et al. (1994); McGill et al. (1997); for the direct detection technique, and Delville (1996) and Drobinsky (1998), for the 10 µm heterodyne detection technique. In addition, airborne measurements have been conducted using a 10 µm heterodyne detection lidar by Werner et al. (2001); Reitebuch et al. (2001, 2003), and more recently for a 0.355 µm direct detection lidar by Reitebuch et al. (2009) and Marksteiner et al. (2011). However, back in 1999 the selection of the ESA's ADM/Aeolus mission was based on the comprehensive comparison reported by Delaval et al. (2000a,b), of the various lidar techniques with radio sounding and 72-MHz radar. The 0.355 µm direct detection Doppler wind lidar developed by the University of Geneva (UoG) was on site but still under testing and not officially involved. Nevertheless, the comprehensive inter-comparison of different lidar techniques presented in the present paper may be useful in future ESA's ADM-Aeolus validation campaigns.

We report the performances of the 0.355 µm direct detection Doppler wind lidar developed at the University of Geneva (UoG), and then the inter comparison with two other wind lidars: 0.532 µm direct detection and 10.6 µm heterodyne detection, and 72-MHz radar. The field campaign took place at the Haute Provence Observatory (44° N, 6° E) in France, in July 1999 (Delaval et al., 2000a,b). The three wind lidars were operated side by side. The 10.6 µm heterodyne lidar was designed and operated by Laboratoire de Météorologie Dynamique (Delville, 1996; Drobinski et al., 1998), the 0.532 µm direct detection lidar was designed and operated by Service d'Aéronomie (Chanin et al., 1989; Garnier and Chanin, 1992). One objective is to compare the performances of the different lidar techniques in various meteorological conditions, to demonstrate that the retrieved wind velocities are the same (within the statistical error) and to explain the differences in complex situations.

AMTD
6, 4551–4575, 2013

2 UoG's 0.355 µm DD wind lidar

University of Geneva developed in 1999 the first direct detection UV-lidar prototype (Flesia et al., 1999) based on molecular backscattered signal from air. The Fabry Perot etalons bandwidths or so-called edges are symmetrically located respect to the laser frequency (Fig. 1). Aerosols backscattered signal contaminates the molecular technique and the two signals should be treated independently in the analysis. However, locating the bandwidth (Fig. 1) in a crossover region of the spectrum where the fractional change in measured molecular and aerosol signals are equal for a given frequency shift, desensitizes the measurement to aerosol scattering (Flesia et al., 1999). Some preliminary measurements were performed at UoG showing a good agreement in the 2–10 km altitude range with the Payerne radiosounding located 60 km east of Geneva (Flesia et al., 2000).

The UoG instrumental parameters are summarized in Table 1.

The wind velocity profile is retrieved assuming that the vertical velocity contribution is negligible respect to the horizontal wind velocity. For calibration purpose, during the wind measurements, the vertical direction is sounded on 10 min basis. Full explanation on the retrieval method can be found in Flesia et al. (1999). The wind profile $V(r)$ at range gate r is retrieved as:

$$V(r) = \frac{1}{\vartheta}\left[\frac{R(r) - R_{\text{vert}}(r)}{R_{\text{vert}}(r)}\right] \quad (1)$$

where $R(r)$ and $R_{\text{vert}}(r)$ represent the ratio of the intensities in the two Fabry–Perot etalons at each range bin r in the slant and vertical directions respectively, and ϑ is the sensitivity of the system.

AMTD
6, 4551–4575, 2013

3 Field campaign

The field campaign took place at the Observatoire de Haute Provence (OHP, 44° N, 6.2° E, 650 m altitude) in southern France from 12 to 23 July 1999 (Delaval et al., 2000a,b).

3.1 Instruments overview and objectives

The wind velocity retrievals from the 0.355 µm Doppler lidar are compared with measurements from the following Doppler lidars:

– A 0.532 µm direct detection double Fabry–Perot Doppler lidar (DC-DDL).

– A 10.6 µm heterodyne detection Doppler Lidar (HDL). The transportable wind lidar is based on a pulsed single longitudinal mode TE CO_2 laser transmitting 300 mJ in a pulse length duration of 2.5 µs at a 10 Hz pulse repetition frequency. The shot to shot frequency fluctuation is about 5 MHz, the measured spectral bandwidth is less than 0.8 MHz. The atmospheric signal is photo-mixed with the beam of a Continuous Wave CO_2 laser (used as local oscillator). A 17 cm telescope collects the atmospheric signals. All lidar signals are processed as independent realizations, and then the frequency estimations can be accumulated to improve the overall performances. The lidar line of sigh can be scanned or pointed in any direction.

The 0.532 µm DC-DDL had been operated on a regular basis at OHP since the early 1990's at Haute Provence Observatory (Souprayen et al., 1999a). The system was designed for nighttime operations to cover the stratosphere and upper troposphere above 8 km. The characteristics of the double Fabry–Perot etalons were chosen to minimize the sensitivity (Chanin et. al, 1994) to particle scatterings (Souprayen et al., 1999b). The instrument was modified for the campaign to allow both nighttime and daytime operations from about 2 to 20 km altitude.

AMTD
6, 4551–4575, 2013

The wind velocity estimates performed by the different Doppler lidars are evaluated with respect to:

1. Two radiosoundings:
   - Ad-hoc radiosounding launches on OHP site during the lidar measurement periods.
   - Radiosoundings launches daily at Nimes station (about 100 km south-east of OHP) at 12:00 and 23:00 UTC.
2. OHP radar
   - VHF 72-MHz stratospheric-trospospheric radar.
3. Numerical weather prediction models
   - ECMWF run at 12:00 and 18:00 UTC.

The main technical characteristics of each instrument and their respective spatial–temporal resolutions are summarized in Table 2.

It can be noticed that the vertical resolution varies as a function pulse length and line-of-sight.

The main objective of the campaign was to assess the performance of Direct Detection Doppler Lidar in cloudy and clear air conditions with respect to GPS radiosoundings taken as a reference. Another objective was to evaluate the relative contributions of instrumental error and representativeness errors.

The Direct Detection 0.355 and 0.532 µm lidars are sensitive to small particles (size with respect to the wavelength) and molecules while the 10.6 µm lidar relies on bigger particles. Aerosols and clouds strong backscattered signal saturates the detectors used in photon counting mode implemented for weak signals from molecules. The 72-MHz radar wavelength is of the order of 4 m, and then the effective scatters are turbulence clusters of the order of 2 m. The ST-Radar measurements are limited in presence of laminar flow.

Discussion Paper | Discussion Paper | Discussion Paper | Discussion Paper |

AMTD

6, 4551–4575, 2013

0.355 µm direct detection wind lidar under testing during a field campaign

S. Lolli et al.

3.2 Atmospheric measurements

The line-of-sight of the each lidar system was fixed at a 40° zenithal angle for each data set and alternately switched from the east to the north directions. The 72-MHz radar had a nonflexible measurement configuration. It was taking measurements at 15° elevation angle in four directions plus the zenith direction. Thus it enabled to retrieve the two horizontal wind components and the vertical wind velocity (Delaval et al., 2000a,b). Balloon radiosondes with GPS tracking system were launched during every set of measurements.

Twelve datasets are chosen for the comparison, as reported in Table 3. Measurements were taken in different atmospheric conditions: clear sky, strong winds, and high aerosol loading. It is important to stress that the retrievals from each instruments had to be provided only few hours after measurement periods to conduct a blind comparison.

4 Methodology for comparison between wind sensors

To quantify the difference between wind profiles, two criteria are chosen:

- a cross-correlation coefficient (CC)
- the Root Mean Square Error (RMSE).

The CC coefficient compares the profile shapes two by two, whereas the RMSE calculates the average absolute value of the difference in wind velocity.

AMTD
6, 4551–4575, 2013

4.1 Cross correlation coefficients

The cross-correlation coefficient between two wind profiles measured by two instruments having the same spatial resolution is:

$$C = \frac{\frac{1}{n}\sum_i \left(x_i - \overline{X}\right)\left(y_i - \overline{Y}\right)}{\sigma_x \sigma_y} \tag{2}$$

where n is the total number of range bins of the X and Y wind velocity profiles, x_i and y_i are the ith value of X and Y, respectively, $\overline{X}$ and $\overline{Y}$ are the respective average values of X and Y variables over the n considered values, and σ_x, σ_y are the standard deviations of the X and Y variables over the n considered values, respectively.

If the cross-correlation coefficient is equal to +1, the fluctuations around the mean value are the same for the two profiles; if it is equal −1, the fluctuations are in opposite direction around their own value; if it is 0 the fluctuations are randomly distributed around their own average value. The cross-correlation coefficient, to be significant, should be calculated over a large number of points. We consider wind profiles with at least 20 points measurements.

4.2 Root Mean Square Error

The Root Mean Square Error is the average absolute value of the difference of wind velocity estimates between two profiles. It is calculated as the difference between the X wind profile and the Y wind profile values, each squared and then averaged over the total range bins. Finally the square root of the average is taken (Eq. 3):

$$\Delta V(X,Y) = \sqrt{\frac{\sum_{i=1}^{n}(x_i - y_i)^2}{n}} \tag{3}$$

where $\Delta V(X,Y)$ is the average deviation between the two wind profiles and x_i, y_i are the wind speed at ith bin and n is the total number of range bins.

Discussion Paper | Discussion Paper | Discussion Paper | Discussion Paper |

AMTD

6, 4551–4575, 2013

0.355 µm direct detection wind lidar under testing during a field campaign

S. Lolli et al.

5 Results

For each set of measurements, the on site radio sounding is taken as the reference for the atmospheric wind velocity profile. Then, the CC coefficients and RMSE are calculated for each instrument. The instrument profiles are interpolated on the same spatial resolution.

5.1 Cross-correlation coefficient

The results in Table 4 show a very good agreement for the average cross correlation coefficients are close to "+1" for each instrument (Table 3). The wind profiles retrieved by lidars and radar display the same shape as the balloon wind profile, even if, under strong wind conditions, the balloon can drifted away from the site.

The correlations are better in the east direction than in the north direction. An explanation is the location of the Haute Provence Observatory site with respect to a valley oriented in the east–west direction, surrounded by two hills, the "Lure" to the north and the "Luberon" to the south. The wind fluctuations due to orography are then more likely meridional than zonal especially in strong wind conditions (Mistral) as shown in Fig. 3. The effects are expected to be stronger in the lower atmosphere (0–5 km). The instrument spatial resolution is an important variable, especially in the lower troposphere, where atmospheric layers are thin. For these reasons, the remote sensors sometimes do not follow the wind fluctuations.

5.2 Root Mean Square Error

Table 5 shows an average absolute deviation between 1.7 and 3.7 $m\,s^{-1}$. Compared with the cross-correlation coefficients, there are not significant discrepancies between north and east LoS. Table 5 also shows, for each instrument the uncertainty on wind velocity retrievals for the time resolution at which lidar measurements were taken. These values can be found in literature (Souprayen et al., 1999a,b; Delville, 1996; Dobinski

AMTD
6, 4551–4575, 2013

et al., 1998; Flesia et al., 2000). The results show that the 10.6 µm HDL-LDM is more precise, at lower altitudes. As shown in Fig. 5, the 0.532 µm lidar has bias substantially higher, due to the detector saturation caused by aerosols in the boundary layer.

The absolute deviation cannot be explained by the instrumental error. Multi-factorial causes may explain this bias. Common to all instruments is the influence of topography, especially for LoS toward the north, then the range resolution are not the same, and different volumes are sounded, especially for the Radar-ST and RS (the balloon can drift away from the site due to strong winds, cf. Fig. 2).

The 0.355 µm lidar seems to be sensitive to a contamination from aerosols and clouds. Even if, as stated in Flesia et al. (1999), the etalons are located in a crossover region where the sensitivity to the molecular signal is equal to the aerosol signal, the cross-over region is not unique, but depends on aerosol or cloud type and on atmospheric conditions such as temperature and humidity. During the field campaign, the 0.355 µm lidar was optimized for an altitude of 5 km by setting up the crossover region, i.e. the distance between the Fabry–Perot bandpasses and the laser line, at 3.32 times the half-width at half height of the bandpasses (Flesia et al., 1999). In Fig. 4, for 21 July 1999, both north and east LOS show an absolute deviation at lower altitudes bigger than instrumental error (east: around 2 and 4 km, north: around 2, 3 and 4.3 km). In this case, the atmospheric condensation at dusk changes both the aerosol microphysics and optical properties, due to higher humidity.

5.3 Discrepancies observed

On 22 July 1999 there was a strong north surface wind (Mistral), clearing the air of particles. Figure 5 shows that the agreement is very poor in wind estimates. Strong winds were inducing gravity waves at low altitudes with significant vertical velocity. As said before, for calibration proposes, it has been assumed negligible. This biases the horizontal wind velocity estimates. A very large discrepancy between the remote sensors and RS is present around 10 km (a difference of about 22 $m s^{-1}$). This is due to the fact that the communication with RS was lost between 8 and 10 km. On this day, the RS wind profile is reliable.

A large number of discrepancies are observed at altitudes close to the tropopause (9–13 km altitude) during jet-stream episodes, between the ST-Radar, 0.532 µm and 0.355 µm lidar instruments. This is visible especially on the dataset V2.20 east LoS, on 22 July 1999 (Fig. 5, bottom panel). These discrepancies put in evidence the issues due to spatial and temporal representativeness of the RS wind velocity retrieval.

6 Conclusions

The UoG's 0.355 µm wind Doppler lidar (Flesia et al., 2000), was deployed at the Haute Provence Observatory in July 1999 with 2 Doppler lidars, a 72-MHz radar and GPS radiosoundings. Twelve datasets with large number of measurements points and different atmospheric conditions (clear sky, clouds, strong wind, high aerosol loading . . .) enable to perform a comprehensive comparison of wind velocity measurements in the same atmospheric conditions. The comparison put in evidence a good agreement between 0.355 µm lidar and radiosounding wind profiles, both in cross-correlation coefficient (average value of 0.78) and average bias (3.67 $m s^{-1}$). The cross-correlation coefficients for all instruments are showing a better agreement to the east than to the north direction, especially in the lower troposphere. This is explained by the topography where the Haute Provence Observatory is located. The absolute deviation is not completely explained by the instrumental error. It can be explained by different probed volumes, as the RS drifted far away from the launching pad and local topography. The Mie backscattering from aerosols and clouds contaminates the 0.355 µm lidar wind velocity measurements. Even though the Fabry–Perot interferometer was designed to eliminate this effect by defining a so-called cross-over region (Flesia et al., 1999), the cross-over region is not unique but depends on particle loading and atmospheric conditions i.e. temperature and humidity. For this campaign, the system was optimized for standard atmospheric conditions expected at 5 km altitude. The comprehensive inter-comparison

AMTD
6, 4551–4575, 2013

of different lidar techniques will be useful in future ESA's ADM-Aeolus validation campaigns to be conducted with all kinds of wind instruments i.e. GPS radio-soundings, in-situ probes, active and passive remote sensors.

Acknowledgements. Special thanks to, C. Hirt (Université de Genève), R. Wilson (radar ST) and OHP personnel for hosting the campaign and for the technical support. The data sets for the 10 µm lidar and 0.532 µm are from a data base built under ESA support.

The publication of this article is financed by CNRS-INSU.

References

Chanin, M.-L., Garnier, A., Hauchecorne, A., and Porteneuve, J.: A Doppler lidar for measuring winds in the middle atmosphere, Geophys. Res. Lett., 16, 1273–1276, 1989.

Chanin, M.-L., Hauchecorne, A., Garnier, A., and Nedeljkovic, D.: Recent lidar developments to monitor stratosphere-troposphere exchange, J. Atmos. Terr. Phys., 56, 1073–1081, 1994.

Courtier, P., Gauthier, P., Rabier, F., Flamant, P., Dabas, A., Lieutaud, F., and Renault, H.: Study of preparation for the use of Doppler wind lidar information in meteorological assimilation systems, ESA-CR(P)-3453, ESA Publications Division, Noordwijk, 82, 1992.

Delaval, A., Flamant, P. H., Aupierre, M., Delville, P., Loth, C., Garnier, A., Souprayen, C., Bruneau, D., Le Rille, O., Wilson, R., Vialle, C., Rees, D., Vaughan, M., and Hardesty, R. M.: Intercomparison of wind profiling instruments during the VALID field campaign, in: Advances in Laser Remote Sensing, Selected Papers Presented at the 20th International Laser Radar Conference, edited by: Dabas, A., Loth, C., and Pelon, J., Editions de l'Ecole Polytechnique, 91128 Palaiseau Cedex, France, 101–104, 2000a.

Delaval, A., Flamant, P. H., Loth, C., Garnier, A., Vialle, C., Bruneau, D., Wilson, R., and Rees, D.: Performance Validation of Direct Detection and Heterodyne Detection Doppler

WIND Lidars, Final Report VALID, CNRS/IPSL, ESA-ESTEC, 2200 AG Nordwijk, the Netherlands, 76 pp., 2000b.
Delville, P.: Development of a Coherent Doppler Laser Radar: Simulation and experimental studies of the transceiver and the heterodyne receiver, PhD thesis, 179, University Paris 6, France, 1996.
Drobinski, P., Brown, R. A., Flamant, P. H., and Pelon, J.: Evidence of organized large eddies by ground-based Doppler lidar, sonic anemometer and sodar, Bound.-Lay. Meteorol., 88, 343–361, 1998.
Flesia, C. and Korb, C.: Theory of the double-edge molecular technique for doppler lidar wind measurement, Appl. Optics, 38, 432–440, 1999.
Flesia, C., Korb, C., and Hirt, C.: Double-edge molecular measurement of lidar wind profiles at 355 nm, Opt. Lett., 25, 1466–1468, 2000.
Garnier, A. and Chanin, M.-L.: Description of a Doppler Rayleigh Lidar for measuring winds in the middle atmosphere, Appl. Phys. B, 55, 25–40 , 1992.
Gentry, B. and Korb, C. L.: Edge technique for high accuracy Doppler velocimetry, Appl. Optics, 33, 5770–5777, 1994.
Huffaker, R. M., Lawrence, T. R., Post, M. J., Priestley, J. T., Hall Jr., F. F., Richter, R. A., and Keeler, R. J.: Feasibility studies for a global wind measuring satellite system (Windsat): analysis of simulated performance, Appl. Optics, 23, 2523–2536, 1984.
Korb, C. L. and Gentry, B. M.: New Doppler lidar methods for atmospheric wind measurements by the edge technique, in: Conference on Lasers and Electro-Optics, Vol. 7 of 1990 OSA Technical Digest Series, Optical Society of America, Washington DC, 1990, 322–324, 1990.
Korb, C. L., Gentry, B., Li, S., and Flesia, C.: Theory of the double-edge technique for Doppler lidar wind measurement, Appl. Optics, 37, 3097–3104, 1998.
McGill, M., Skinner, W., and Irgang, T.: Validation of wind profiles measured with incoherent Doppler lidar, Appl. Optics, 36, 1928–1932, 1997.
Marksteiner, U., Reitebuch, O., Rahm, S., Nikolaus, I., Lemmerz, C., and Witschas, B.: Airborne direct-detection and coherent wind lidar measurements along the east coast of Greenland in 2009 supporting ESA's Aeolus, in: Proceedings of SPIE Vol. 8182, Lidar Technologies, Techniques, and Measurements for Atmospheric Remote Sensing VII, 81820J, 30 September 2011Prague, doi:10.1117/12.897528, 2011.

AMTD
6, 4551–4575, 2013

0.355 µm direct detection wind lidar under testing during a field campaign

S. Lolli et al.

Reitebuch, O., Werner, C., Leike, I., Delville, P., Flamant, P. H., Cress, A., and Engelbart, D.: Experimental validation of wind profiling performed by the airborne 10 µm-heterodyne Doppler lidar WIND, J. Atmos. Ocean. Tech., 18, 1331–1344, 2001.

Reitebuch, O., Volkert, H., Werner, C., Dabas, A., Delville, P., Drobinski, P., Flamant, P. H., and Richard, E.: Determination of air flow across the Alpine ridge by a combination of airborne Doppler lidar, routine radiosounding and numerical simulation, Q. J. Roy. Meteorol. Soc., 129, 715–728, 2003.

Reitebuch, O., Lemmerz, C., Nagel, E., Paffrath, U., Durand, Y., Endemann, M., Fabre, F., and Chaloupy, M.: The Airborne demonstrator for the direct-detection Doppler wind lidar ALADIN on ADM-Aeolus, Part I: Instrument Design and Comparison to Satellite Instrument, J. Atmos. Ocean. Tech., 26, 2501–2515, 2009.

Souprayen, C. A., Garnier, A., Hertzog, A., Hauchecorne, A., and Porteneuve,. J.: Rayleigh–Mie Doppler wind lidar for atmospheric measurement. I. Instrumental set-up, validation and first climatological results, Appl. Optics, 38, 2410–2421, 1999a.

Souprayen, C. A., Garnier, A., Hertzog, A., Hauchecorne, A., and Porteneuve, J.: Rayleigh–Mie Doppler wind lidar for atmospheric measurements: Part II: Mie scattering effect, theory, and calibration, Appl. Optics, 38, 2422–2431, 1999b.

Stoffelen, A., Pailleux, J., Källen, E., Vaughan, J. M., Isaksen, L., Flamant, P. H., Wergen, W., Andersson, E., Schyberg, H., Culoma, A., Meynard, R., Endemann, M., and Ingmann, P.: The Atmospheric Dynamics Mission for global wind field measurement, Bull. Atmos. Meteorol. Soc., 86, 73–87, 2005.

Werner, C., Flamant, P. H., Reitebuch, O., Köpp, F., Streicher, J., Rahm, S., Nagel, E., Klier, M., Hermann, H., Loth, C., Delville, P., Drobinski, P., Romand, B., Boitel, C., Oh, D., Lopez, M., Meissonnier, M., Bruneau, D., and Dabas, A. M.: WIND Infrared Doppler lidar instrument, Opt. Eng., 40, 115–125, 2001.

Table 1. 0.355 µm technical characteristics.

Laser Wavelength	0.355 µm
Laser energy per pulse	80 mJ
Pulse Repetition Frequency	30 Hz
Laser divergence	0.5 mrad
Telescope diameter	25 cm
Telescope Field of View	0.125 mrad
Etalon Plate spacing	1.25 cm
Effective Finesse	7.7
Etalon spectral bandwidth	1.56 GHz
Number of etalon channels	3
Laser etalon separation-locking ch.	0.78 GHz
Laser etalon separation atm. Ch.	±2.605 GHz

AMTD
6, 4551–4575, 2013

Table 2. VALID-2 instrumental parameters.

Instrument	Range maz.	Spatial Res.	Temporal Res.	Averaged precision
532 nm DD-Lidar OHP	D: 2–20 km N: 2–30 km	115 m	30 min	1.1–3.8 m s^{-1}
10.6 µm DH Lidar LMD	1.5–12 km	250 m	1 min	0.4 m s^{-1}
355 nm DD UoG	1–12 km	380 m	12 min	1.2–3 m s^{-1}
Radar ST 72 MHz	2–15 km	375 m	15 min	N/A

AMTD
6, 4551–4575, 2013

Table 3. Chosen datasets for the intercomparison versus the radiosonde and relative weather conditions.

Set	Date	Starting time UTC	Ending time UTC	Baloon	Direction
V2.4	14 Jul 1999	1500	1600	1521	E clear sky
		1600	1700		N
V2.14	19 Jul 1999	1500	1600	1457	N overcast
		1600	1700		E
V2.17	20 Jul 1999	2230	2315	2241	E clear sky, low clouds
		2315	0000		N
V2.18	21 Jul 1999	2000	2100	2059	N clear sky, foggy
		2100	2200		E
V2.20	22 Jul 1999	2000	2100	2022	N Mistral, clear sky
		2100	2200		E
V2.22	23 Jul 1999	1500	1600	1523	N Mistral, clear sky
		1600	1700		E

AMTD
6, 4551–4575, 2013

0.355 µm direct detection wind lidar under testing during a field campaign

S. Lolli et al.

Table 4. Average cross-correlation coefficients retrieved on selected datasets.

	0.532 µm DC-DDL	0.355 µm DEDG	10.6 µm HDL-LMD	Radar ST
Average value	0.84	0.78	0.87	0.87
Average value N	0.77	0.73	0.82	0.82
Average value E	0.90	0.83	0.92	0.92

AMTD
6, 4551–4575, 2013

Table 5. Average Root Mean Square Error retrieved on selected datasets.

	0.532 µm DC-DDL	0.355 µm DEDG	10.6 µm HDL-LMD	Radar ST
Average value ($m\,s^{-1}$)	3.40	3.67	1.64	2.30
Average value N ($m\,s^{-s}$)	3.99	3.51	1.66	2.25
Average value E ($m\,s^{-1}$)	2.89	3.12	1.63	2.35
Instrumental error ($m\,s^{-1}$)	1.1–3.8	1.2–3	0.4	N/A

AMTD
6, 4551–4575, 2013

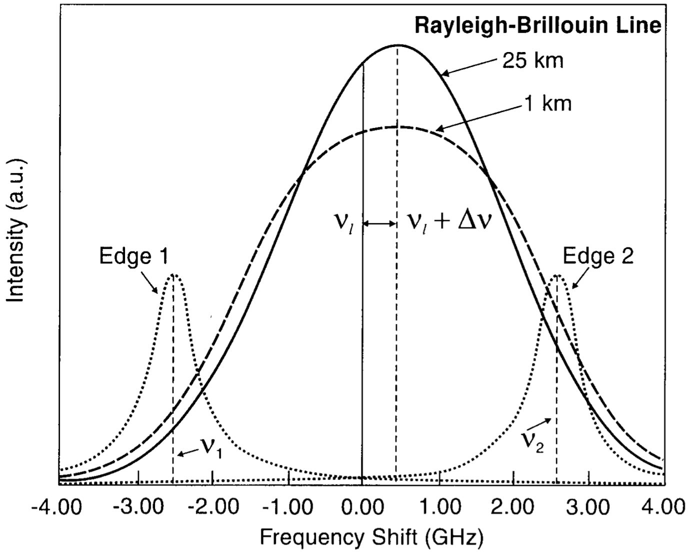

Fig. 1. Measurement of R–B profile frequency shifts with two edge filters located at frequencies ν_1 and ν_2 respect to the laser frequency ν_l (Flesia et al., 1999).

AMTD
6, 4551–4575, 2013

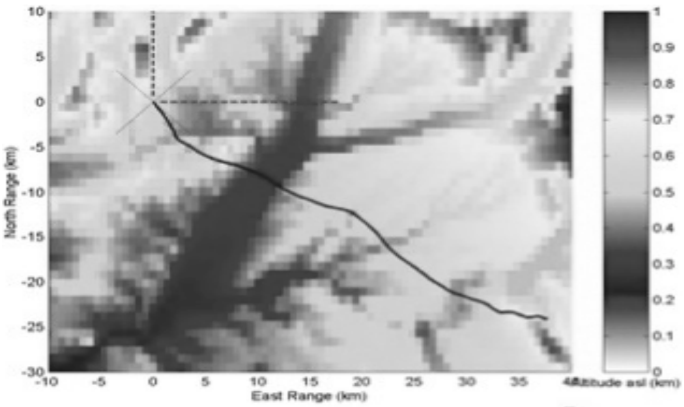

Fig. 2. Balloon trajectory with the topography of the region. The valley effect is clearly visible.

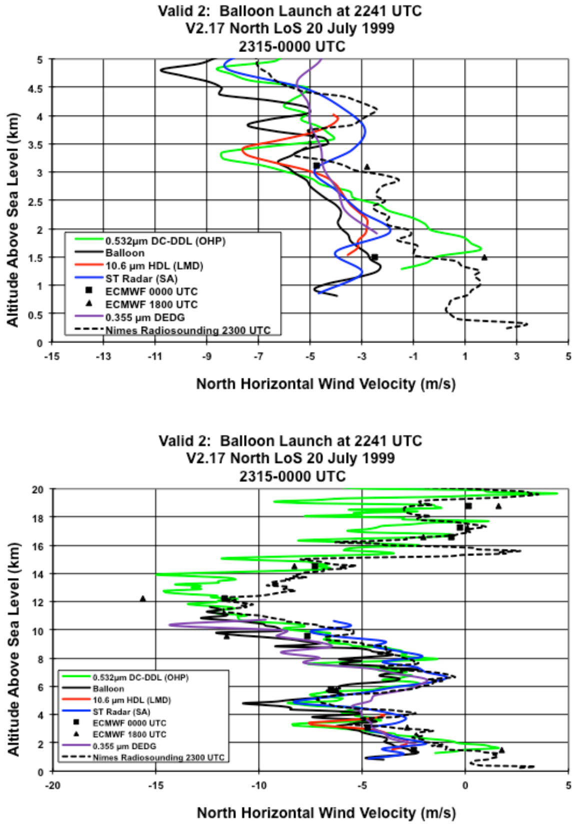

Fig. 3. Strong meridional winds (Mistral) observed on 20 July 1999 between 23:15 and 24:00 UTC by the 0.355 um lidar (purple), the 0.532 um lidar (green), the 10.6 um lidar (red), the ST radar (blue). In black are the ad-hoc balloon radiosounding launched at 22:41 UTC (black, solid line) and the Nîmes radiosounding from 23:00 UTC (dashed line). The triangles and squares are from ECMWF at 18:00 UTC and 00:00 UTC on 21 July, respectively. The top panel is zoomed between 0 and 5 km altitude.

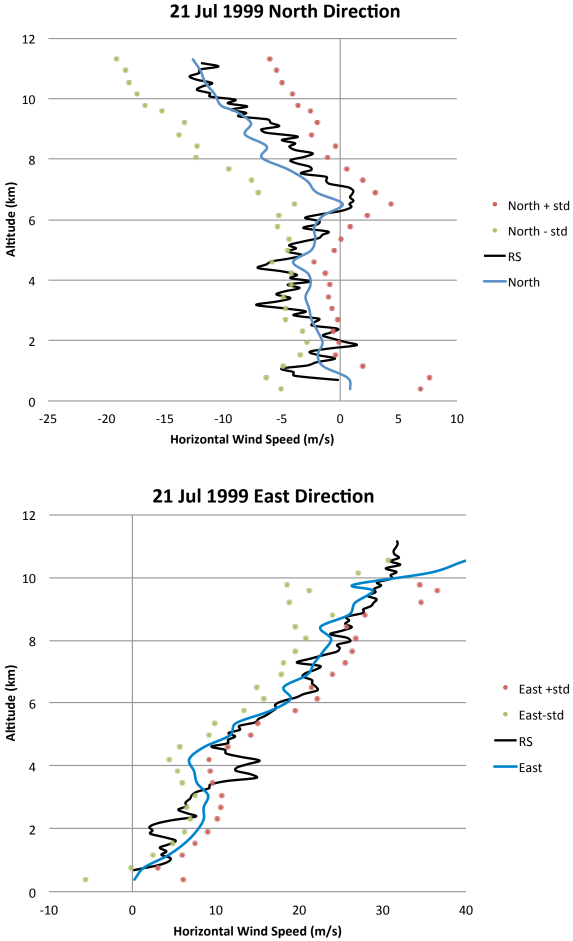

Fig. 4. Wind profiles from the 0.355 µm lidar (mean in blue; mean + standard deviation in red; mean – standard deviation in green) compared with the simultaneous GPS radiosounding (black, launched at 20:59 UTC) on 21 July 1999 for the north (upper panel, 20:00–21:00 UTC) and east (lower panel, 21:00–22:00 UTC) directions.

AMTD
6, 4551–4575, 2013

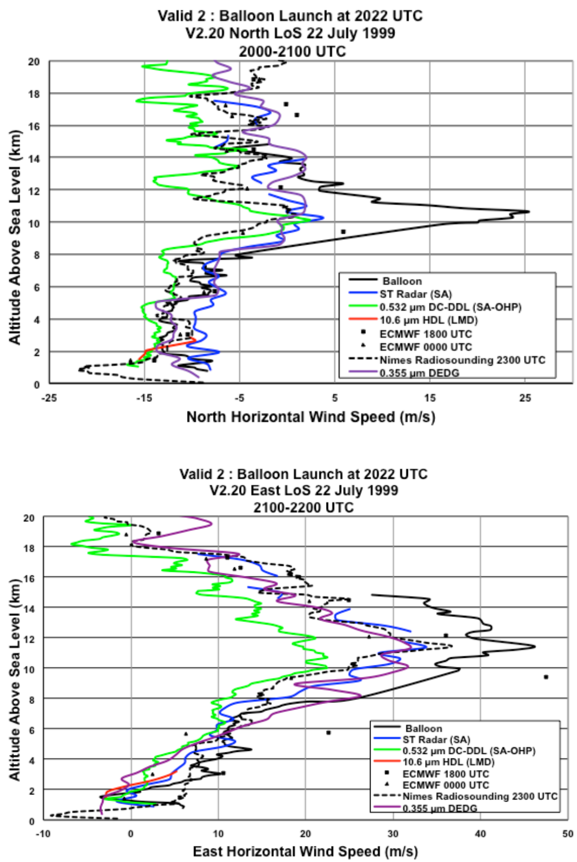

Fig. 5. Wind profiles comparisons on 22 July 1999 with the same presentation as in Fig. 3. Upper panel: north direction between 20:00 and 21:00 UTC; lower panel: east direction between 21:00 and 22:00 UTC, with a strong jet-stream at the tropopause. The ad-hoc balloon radiosounding was launched at 20:22 UTC.

AMTD
6, 4551–4575, 2013

0.355 µm direct detection wind lidar under testing during a field campaign

S. Lolli et al.